Pathological LSD1 mutations repress enhancer-mediated gene regulatory networks in early differentiation

Daria Bunina[1,2,7], Pierre-Luc Germain[3], Alejandro Lopez Tobon[3], Nadine Fernandez-Novel Marx[1], Christian Arnold[2], Andrew Ahern[2], Annique Claringbould[2], Mang Ching Lai[2], Sampath Rangasamy[4], Vinodh Narayanan[4], Peter Lorentzen[5], Karen M. Park[6], Antonio Adamo[3], Giuseppe Testa[3], Judith Zaugg[2,7], Kyung-Min Noh[1,7]

Affiliations

[1] - European Molecular Biology Laboratory (EMBL), Genome Biology Unit, Heidelberg, Germany
[2] - European Molecular Biology Laboratory (EMBL), Structural and Computational Biology Unit, Heidelberg, Germany
[3] - Department of Experimental Oncology, European Institute of Oncology, IRCCS, Milan, Italy
[4] - Center for Rare Childhood Disorders and Neurogenomics Division Translational Genomics Research Institute, Phoenix, USA
[5]- Department of Economics, University of San Francisco, San Francisco, California, USA
[6]- Citizen scientist, San Francisco, California, USA
[7] - corresponding author

Abstract

Lysine-specific demethylase 1 (LSD1/KDM1A) demethylates both histone and non-histone substrates, recruits repressive chromatin complexes, and is increased in cancers. De novo LSD1 mutations impairing protein function lead to a rare developmental disorder, but the molecular details of the pathology remains unclear. Using patient-derived fibroblasts, reprogrammed pluripotent stem cells, and differentiated cells, we found over 4000 differentially expressed genes and 68 transcription factors (TFs) whose motif accessibilities changed upon LSD1 mutation. An enhancer-mediated gene regulatory network approach identified transcriptional repressors with impaired activity in fibroblast and stem cells, leading to erroneous activation of their target genes. We also revealed overall decreases in TF target gene expression during early lineage differentiation of LSD1 mutant stem cells, likely caused by increased activity of repressive histone deacetylases (HDACs), co-factors of LSD1. Indeed, an HDACs inhibitor restored changes in gene expression including downregulation phenotype. Our findings characterize the molecular pathogenesis of LSD1 mutations and suggest potential therapeutic strategies for the developmental disorder and cancers caused by LSD1 dysregulations.

Introduction

Epigenetic modifications on chromatin are essential for regulating cell type specific gene expression and, therefore, normal development. The positioning and dynamics of histone lysine methylation at enhancers and promoters, carried out by lysine methyltransferases and demethylases, is critical for cellular processes, such as transcription[1], DNA repair[2], the cell cycle[3], and differentiation capacity[4]. Lysine-specific demethylase 1 (LSD1, encoded by the KDM1A gene) demethylates histone H3 lysine 4 mono- and di-methylated moieties (H3K4me1/2)[5], marks found at active and poised enhancers and promoters. LSD1 also recruits repressive protein complexes, such as CoREST[6] and NuRD[7], to chromatin. LSD1 has been implicated in the control of cell differentiation[8] and early embryogenesis[9] possibly by silencing active enhancers in stem cells when they undergo differentiation. Functional alterations of LSD1 have been found in pathological conditions, such as hematopoiesis impairment[10] and various cancers[11].

Dominant missense point mutations in LSD1 cause the developmental disorder[12] Cleft Palate, Psychomotor Retardation and Distinctive Facial Features (CPRF), which resembles Kabuki syndrome, characterized by distinctive facial features, muscle and skeletal abnormalities, and cognitive impairment. Three of the pathological mutations (Glu403Lys, Asp580Gly, Tyr785His) in purified proteins have been shown to impair LSD1 catalytic activity and, to varying extents, LSD1 binding to the histone H3 N-terminal tail[13]. LSD1 inactive mutants were also able to recruit corepressors (e.g., CoREST, HDAC1/2) when stably expressed in transfected cells[13]. Nevertheless, the molecular mechanisms by which the LSD1 mutations cause pathological manifestation have not been elucidated in the context of patient cells.

Here, using patient material, we investigated the effects of the pathological mutations Glu403Lys and Tyr785His on chromatin and gene expression in different cell types and across differentiation. We observed widespread misregulation of gene regulatory networks and increased transcriptional repression during differentiation, likely caused by increased activity of LSD1 co-factors, such as HDACs. Treating the cells with an inhibitor of HDACs, an FDA approved drug, rescued the molecular phenotype of the cells. Even with a limited number of patient cases, our integrated data analysis has identified a target pathway that may help treat a rare human disease. Our findings also provide a genome regulatory feature coupled to LSD1 dysregulations that may apply to various cancers.

Results

LSD1^{MUT} impairs chromatin accessibility at regulatory elements

To understand how de novo heterozygous mutations in LSD1 cause CPRF syndrome, we obtained primary skin fibroblasts, which express LSD1 (Extended Data Fig.1a), from two male pediatric patients (family A - Glu403Lys and family B - Tyr785His), and their healthy fathers (Fig. 1a). Given LSD1 largely acts on chromatin at regulatory elements, such as enhancers and promoters, we hypothesized that heterozygous mutant cells would exhibit a disruption of chromatin at regulatory elements. To test this idea, we used ATAC-seq to map chromatin

accessibility at regulatory elements in both the LSD1 mutant ($LSD1^{MUT}$) cells of CPRF patients and healthy fathers (two biological replicates for each condition). A comparison using principal component analysis (PCA) revealed a clear separation of the patient and healthy samples (Fig. 1b). Differential chromatin accessibility analysis identified 16,425 peaks (from a total of 96,467 peaks) that were evenly distributed between less and more accessible in $LSD1^{MUT}$ vs $LSD1^{WT}$ (FDR < 0.05, Fig. 1c). More accessible regions in $LSD1^{MUT}$ are enriched for active and bivalent/poised transcription start sites (+/- 3kb from TSS, 24% of peaks in $LSD1^{MUT}$ vs. 6.5% of peaks in $LSD1^{WT}$) and GC-rich promoter motifs (HOMER motif enrichment tool). In contrast, less accessible regions in $LSD1^{MUT}$ are enriched for active and bivalent enhancers but depleted for the TSS, compared to the background peaks (Extended Data Fig. 1b). These results suggest a broadly impaired chromatin regulatory landscape in $LSD1^{MUT}$.

To examine the involvement of specific transcription factor (TF) binding associated with changes in chromatin accessibility between $LSD1^{MUT}$ and $LSD1^{WT}$, we applied diffTF analysis[14], which quantifies genome-wide differential TF motif accessibility as “TF activity,” with increased TF motif accessibility corresponding to higher TF activity, and decreased accessibility to lower activity. Comparing the TF activities of $LSD1^{MUT}$ and $LSD1^{WT}$, and excluding age-related TFs to minimize the effect of the donors’ age (see Methods), identified 68 significantly changed TFs (Fig. 1d). The 44 TFs with increased activity in $LSD1^{MUT}$ include developmental factors (Tbx3, Mesp1, Hoxb6/a11) and the epithelial-to-mesenchymal transition (EMT) TFs Zeb1 and Snai1, whereas several TFs with decreased activity include the AP-1 complex, which controls responses to various stimuli. Protein-protein interaction data (STRING database) showed greater interconnection between differentially active TFs than expected by chance (average node degree is 3.85 compared to 1.5 in a network of non-significant TFs and protein-protein interaction enrichment p-value is < 1e-16), suggesting that genome-wide chromatin accessibility differences in $LSD1^{MUT}$ are associated with a group of functionally related TFs.

$LSD1^{MUT}$ induced changes in promoter accessibility and expression

Having identified TFs (inferred by motif) that are mis-regulated in $LSD1^{MUT}$, we sought to determine transcriptional changes in fibroblasts. RNA-seq analysis of LSD1 mutants and controls revealed more than 2500 differentially expressed genes (Fig. 1e), of which 1488 were upregulated and 1178 downregulated in $LSD1^{MUT}$ (DESeq2, FDR < 0.1, Fig. 1f). Up-regulated genes were enriched for cell cycle transition and DNA replication GO terms (Fig. 1g), however upregulation of cell cycle genes appeared in only one (Glu403Lys) of the two $LSD1^{MUT}$ samples, undermining its wide relevance in CPRF syndrome. The LSD1 Glu403Lys mutant, but not Tyr785His mutant, showed a strong impairment in histone H3 binding[13], which could decrease localization of repressive co-factors, resulting in upregulation of target genes. Down-regulated genes in $LSD1^{MUT}$ were enriched for the extracellular matrix, inflammatory response, and angiogenesis GO terms, consistent with the role of extracellular matrix in the EMT and impairment of the repressive EMT TFs Zeb1 and Snai1 identified in the diffTF analysis.

To assess the relationships between chromatin accessibility and gene expression changes in $LSD1^{MUT}$ fibroblasts, we linked each ATAC-seq peak at promoter region to the gene and analyzed these peak-gene links (Fig. 1h). We observed a positive correlation between

significant differential chromatin accessibility and gene expression (Pearson's coefficient = 0.45). Top correlated links appear in RBM46, DDX43, and TLR4 genes. Yet, the numbers of linked cases (n=322) were low and limited to the promoter peak-gene links, indicating that a more robust approach is required to analyze the functional interactions between changes in chromatin accessibility and gene expression.

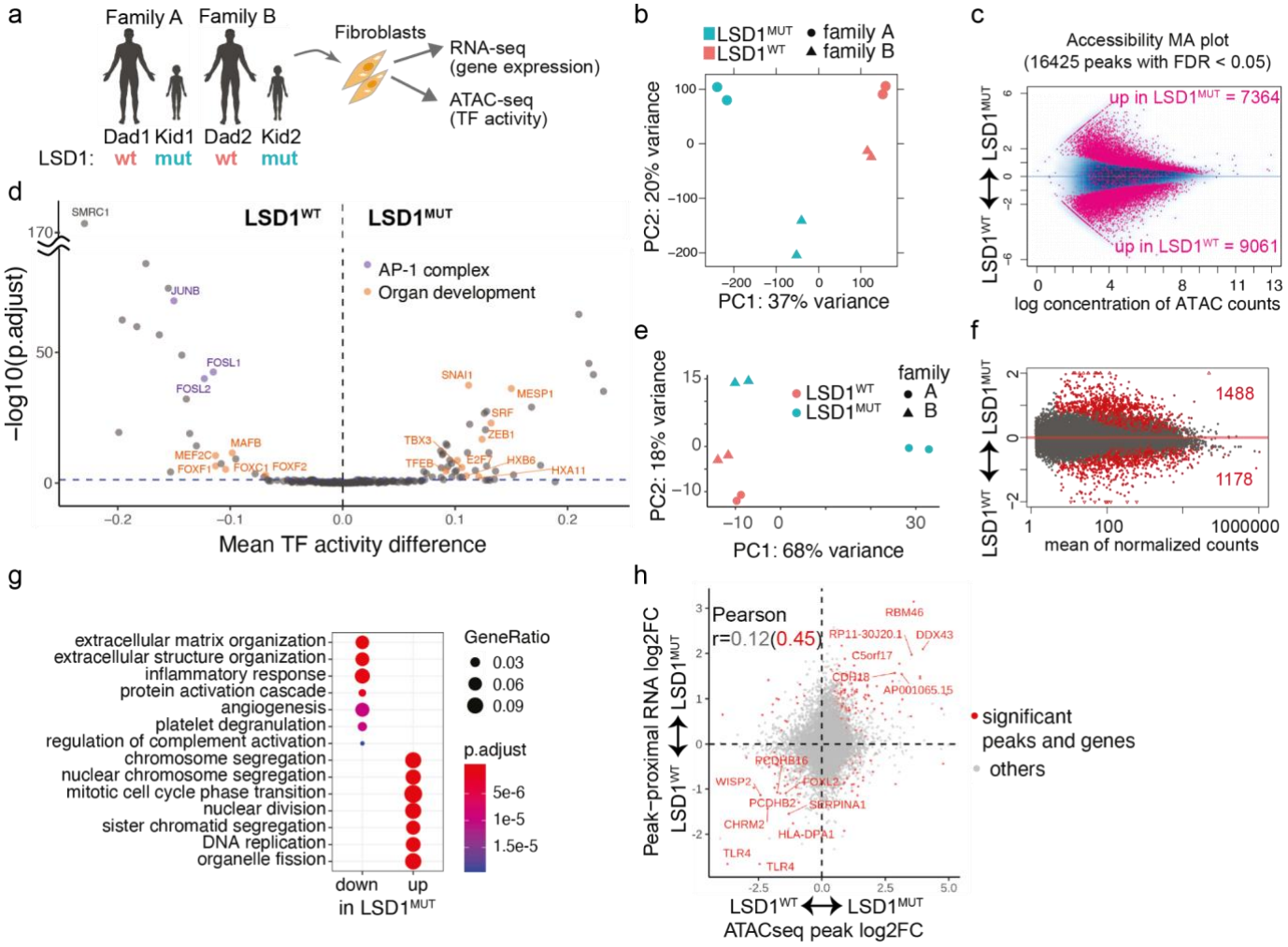

Figure 1. Effects of LSD1 mutation on chromatin accessibility and gene expression in fibroblasts. a) Schematic of the experimental set-up. b) Principal component analysis (PCA) plot of ATAC-seq peak accessibility data in primary fibroblasts. Principal components 1 and 2 are shown together with the variance they explain. c) Differential accessibility analysis with MA plot showing the concentration of accessible fragments in the ATAC-seq peaks against log2 fold change of peak accessibility in $LSD1^{MUT}$ vs. $LSD1^{WT}$. Significantly differential peaks (FDR < 0.05) are marked in pink. For panels c,d,f: n=4 for each condition (2 families, each 2 replicates). d) Differential TF activity analysis in primary fibroblasts comparing healthy controls ($LSD1^{WT}$) vs patients with $LSD1^{MUT}$. TFs colored by "AP-1 complex" (purple) and GO term "Embryonic organ development" (orange). e) PCA plot of RNA-seq data in fibroblasts. f) Differential expression analysis in fibroblasts with MA plot showing average normalized gene expression values against log2 fold change in gene expression. Significantly differential genes (FDR < 0.1) are shown in red. g) gene ontology enrichments of significantly differential genes in fibroblasts. h) Scatter plot showing correlations between ATAC-seq peak accessibility and gene expression changes in $LSD1^{MUT}$, where peaks were linked to the nearest gene within 3 kb from the transcription start site. Significantly differentially accessible peaks and differentially expressed proximal genes are shown in red.

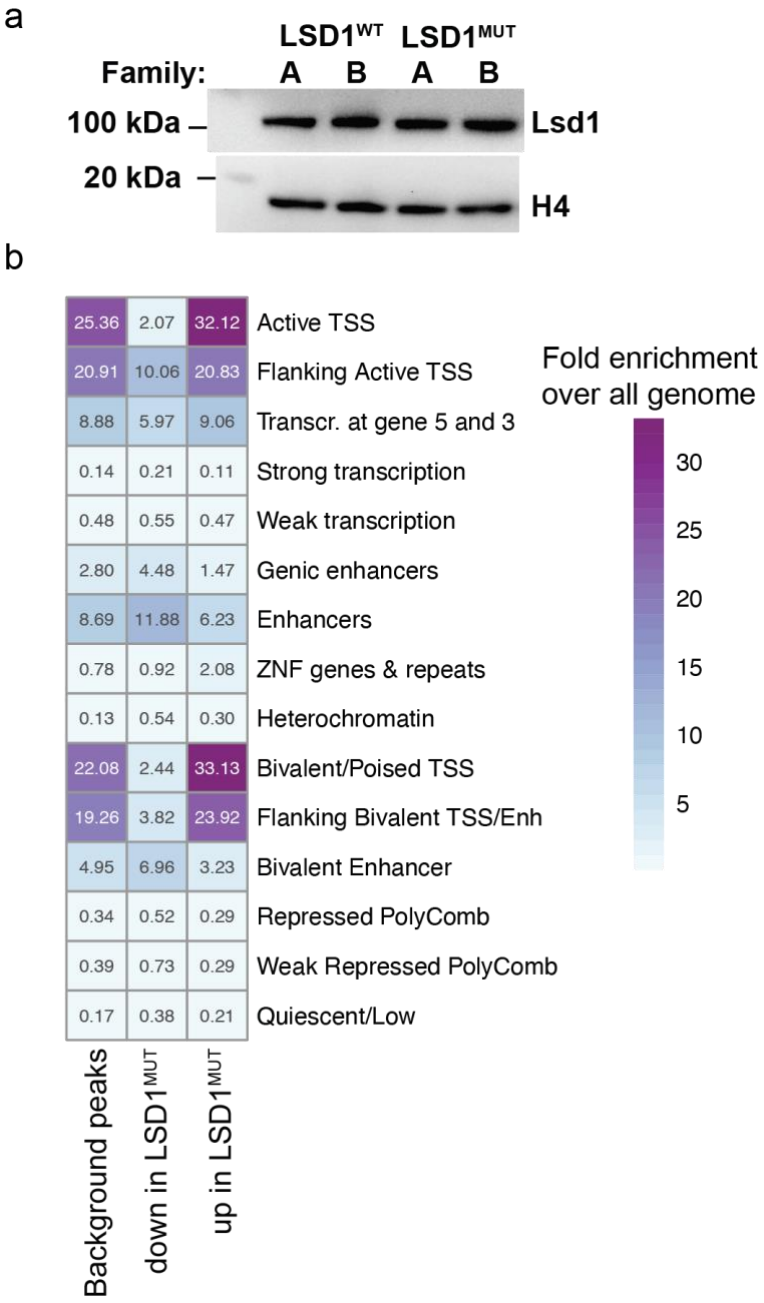

Extended Data Fig.1. a) Western blot of nuclear extracts from primary fibroblasts showing Lsd1 protein expression (92 kDa size) across samples and replicates. b) Enrichments of non-differential ATAC-seq peaks and significantly up- or down-regulated peaks in LSD1^{MUT} in 15 chromatin states identified in the Roadmap epigenome project for foreskin fibroblasts (E055). Fold enrichments relative to the whole genome background were calculated with ChromHMM software http://compbio.mit.edu/ChromHMM/.

TF-gene modules affected by LSD1^{MUT}

To dissect the link between changes in chromatin accessibility at regulatory elements and gene expression beyond simply proximity, and to connect changes in TF activity with downstream effects on target gene expression, we constructed an enhancer-mediated gene regulatory network (eGRN) based on co-variation across samples with paired RNA-seq and chromatin

activity readout [15, 16] such as ATAC-seq data (Kamal et al, in preparation). We calculate correlations across samples between TF expression and ATAC-seq signal at their binding motifs (TF-to-peak correlations), and between ATAC-seq peaks and RNA expression of nearby genes (peak-to-gene correlations, Fig. 2a and Methods) to connect the genes to their putative regulatory elements and TFs. To obtain the TF-enhancer-gene links in the cell types relevant for the LSD1^{MUT} and CPRF syndrome phenotype, we used published datasets from healthy brain samples, two independent studies on a differentiation time course spanning pluripotent stem cells, via mesoderm, to cardiomyocytes, in addition to our fibroblast data, containing paired ATAC- and RNA-seq data (Table 1). After filtering for significant TF-to-peak and peak-to-gene connections, we obtained a network of 393 TFs linked to 15,128 unique genes via 506,564 regulatory elements (Fig. 2a and Methods). This large network represents the global set of all TF-target gene connections in healthy cell types. In this eGRN, only 13% of peaks were linked to the nearest gene, consistent with our previous study reporting <20% of linked peaks[15]. The majority of peaks were linked to distal genes rather than the nearest gene within 500 kb of the TSS (Fig. 2B), implying greater regulatory network complexity and the relevance of using cell type specific ATAC- and RNA-seq data to derive peak-gene connections.

Source	# samples	Type	Link
This study	8	Fibroblasts	
Snyder/Murry lab	40	hiPSC, mesoderm, cardiac mesoderm, cardiomyocyte	https://www.ncbi.nlm.nih.gov/geo/query/acc.cgi?acc=GSE106690; https://www.ncbi.nlm.nih.gov/geo/query/acc.cgi?acc=GSE85332
PsychENCODE	11	Brain	https://www.synapse.org/#!Synapse:syn7062404 https://www.synapse.org/#!Synapse:syn7349497

Table 1.

We defined the genes connected to each TF in the eGRN as TF regulons (TF-gene modules). For each TF, we assessed whether its regulon activity, i.e. the distribution of aggregated expression changes of all TF target genes compared in LSD1^{MUT} vs. LSD1^{WT} fibroblasts, was significantly different from the expression changes in all other genes (see Methods and Extended Data Fig. 2a). Globally the distribution of gene expression of all 15,128 genes retained in the eGRN was not affected by LSD1^{MUT} (mean log2 fold changes are centered around 0, Extended Data Fig. 2b), however we found >100 TFs whose regulons' expression (log2 fold change in LSD1^{MUT} vs. LSD1^{WT}) in fibroblasts deviated significantly from the background (Fig. 2c). Many of these regulons were upregulated in LSD1^{MUT} fibroblasts, consistent with an overall de-repression of genes due to reduced LSD1 function and perturbed repressor TF activity, as seen in the de-repression of the ZEB1 and GLIS1/2/3 regulons (Fig. 2c). The differential activity of this set of TFs, based on ATAC-seq data, correlates with the activity of their regulons from the eGRN (pearson correlation: 0.5, Extended Data Fig.2c),

confirming the direct effects of LSD1^{MUT}-mediated TF motif accessibility disruption on TF target gene expression. Our eGRN therefore identified a specific set of TFs (inferred by motif) that likely mediate the changes in gene expression in LSD1^{MUT} fibroblasts, with many of these changes being upregulation of genes.

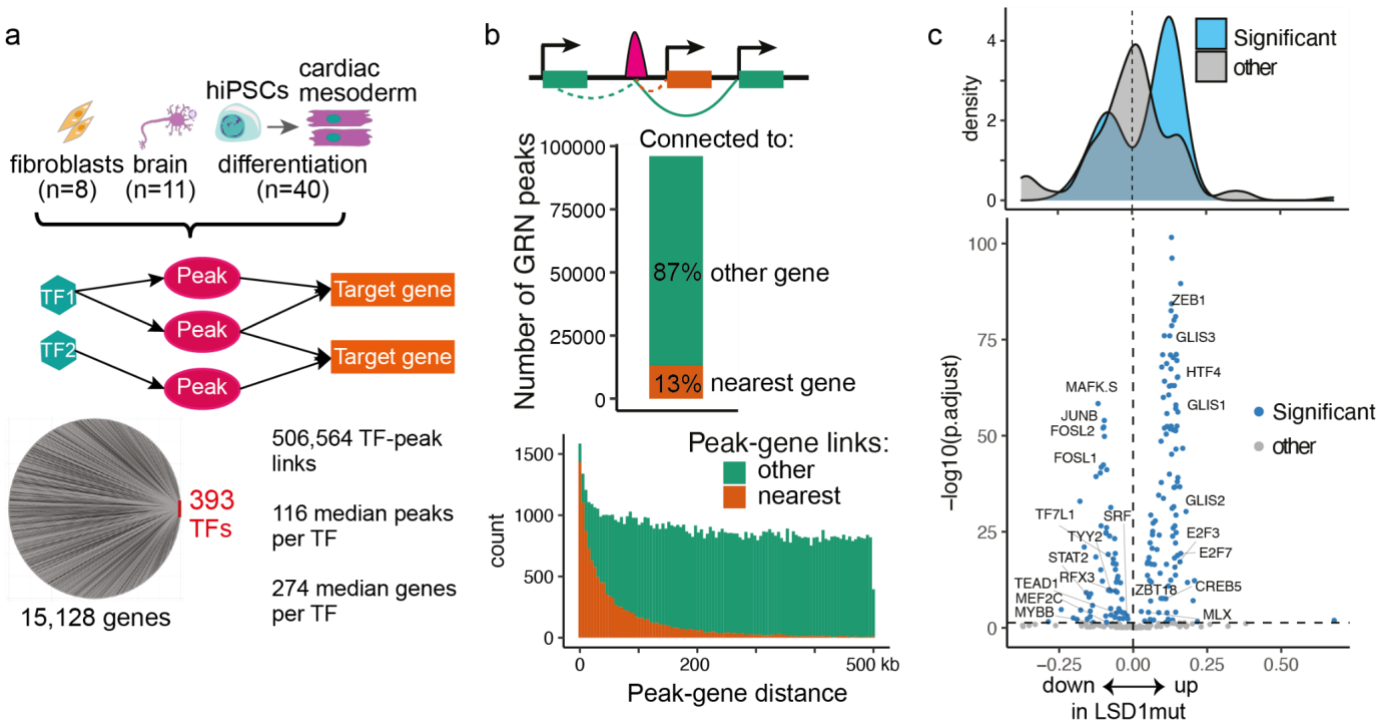

Figure 2. Construction of eGRN using paired ATAC- and RNA-seq from different cell types. a) Schematic of the eGRN connecting TFs and their target genes through enhancers. eGRN statistics of the network resulting from healthy samples across 6 cell types and differentiation states (Table 1). b) Top schematic: solid green line but not dotted lines shows correlated peak-gene links present in the eGRN. Middle panel: percentage of eGRN peaks linked to the nearest gene or to the other gene, from the total of 96,050 peaks. Bottom panel: the distribution of distances between peak and gene in the eGRN, colored by peaks linked to the nearest gene or other gene. c) For each TF, the mean differential expression in fibroblasts (LSD1^{MUT} vs LSD1^{WT}) of its target genes (=TF regulons) is shown as a volcano plot, and a density plot stratified for significant (blue) and non-significant (grey) TF regulons.

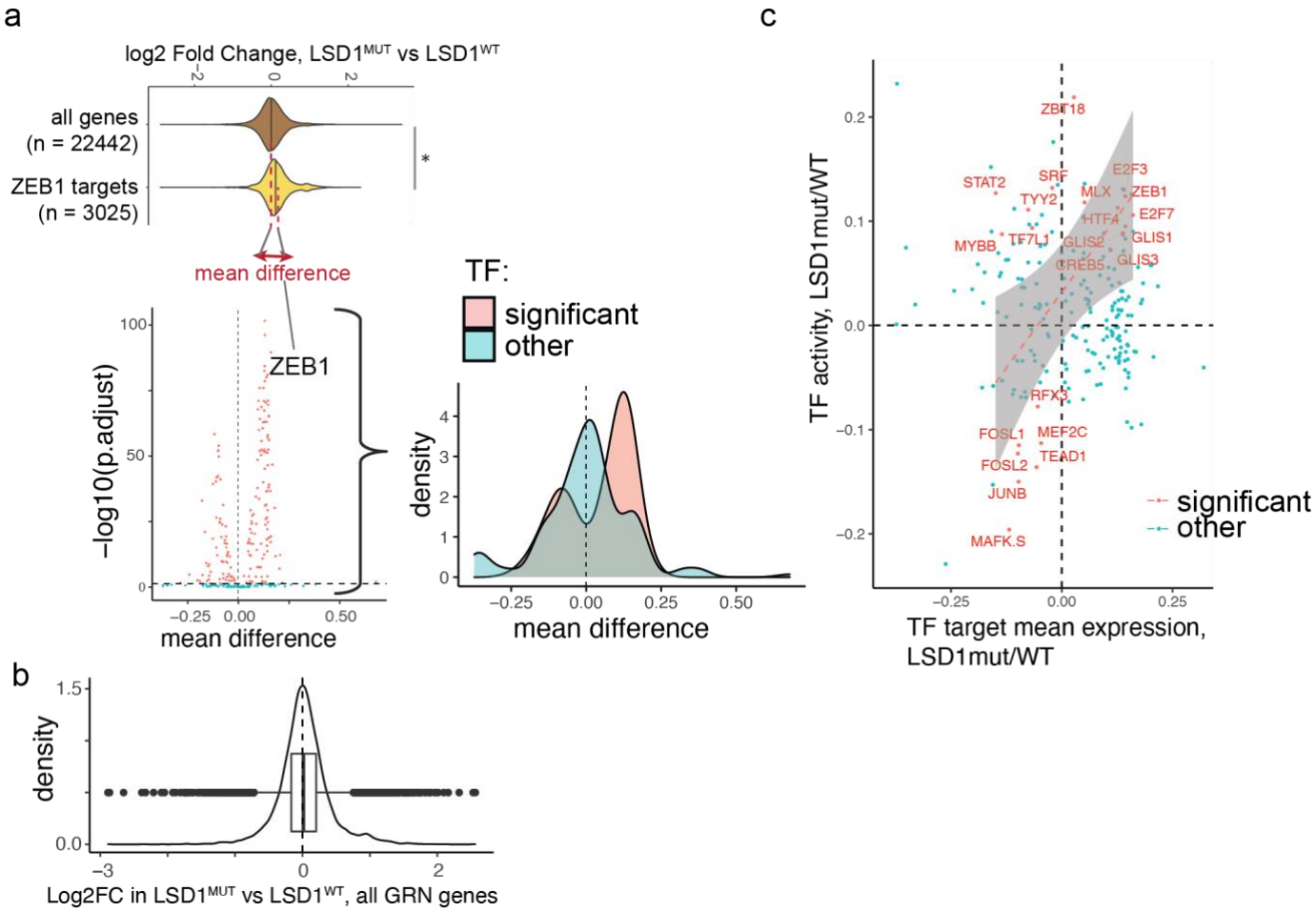

Extended Data Fig.2. a) Violin plot showing that expression of ZEB1 regulons (its target genes) is on average increased compared to all expressed genes in fibroblasts and the difference is calculated as mean(ZEB1 regulon) - mean(all genes). Mean difference for each TF regulon is shown below as volcano plot against adjusted p-value. The distributions of the significant and other TFs are visualized by density plot. b) Distribution of gene expression of all unique genes in the GRN in fibroblasts ($LSD1^{MUT}$ vs $LSD1^{WT}$). c) Scatter plot showing correlation of TF activity (defined by diffTF) and TF regulon expression (defined in panel A).

Gene expression during lineage differentiation in $LSD1^{MUT}$

The role of LSD1 in disabling enhancer regions through the removal of H3K4me1/2 marks is critical during cellular differentiation, when the enhancer landscape has to be re-established[17]. To study the differentiation of patient-derived cells, we reprogrammed patient- and control-derived primary fibroblasts from the two families into human induced pluripotent stem cells (hiPSCs). All hiPSC clonal lines (n= 3 from family A and n = 2 from B, $LSD1^{WT}$; n = 2 from family A and n = 2 from B, $LSD1^{MUT}$) show normal chromosome numbers, intense staining of pluripotency markers (e.g., Oct4, SSEA-4, TRA-1-60), and high expression levels of pluripotency marker genes (Extended Data Fig.3a). We differentiated all nine hiPSC lines into three main embryonic lineages: endoderm, mesoderm, and the neuronal lineage, and analyzed the effects of $LSD1^{MUT}$ on gene expression (Fig. 3a-b). In the pluripotent state, we observed limited changes in gene expression between $LSD1^{MUT}$ and $LSD1^{WT}$ (58 differentially expressed

genes, Fig. 3c) partially due to the high variability between the hiPSC lines (Extended Data Fig. 3b), reminiscent of other reprogrammed hiPSC studies[18]. However, during differentiation into the three lineages, LSD1^{MUT} had a substantial impact on gene expression. Over 4700 genes were differentially expressed in endoderm, over 1600 in the neuronal lineage, and over 700 in mesoderm (FDR < 0.05, Fig. 3c), consistent with the phenotype of the affected patients who show symptoms related to all lineages (e.g., developmental delay, muscle hypotonia, distinctive facial features). While most of the differential genes were mis-regulated in only one of the cell lineages, a larger set (596 genes) were mis-regulated in both endoderm and neuronal lineages, and 87 genes were mis-regulated in all three lineages.

We observed that genes downregulated in endoderm and neuronal lineages were enriched in cell cycle related GO terms (DNA replication, sister chromatid segregation, Extended Data Fig. 3c). Unlike the increase in cell cycle genes observed in one of the two LSD1^{MUT} individuals in primary fibroblasts, the downregulation of cell cycle related genes across differentiating lineages occurred in both LSD1^{MUT} samples, implying more relevance to CPRF syndrome. Differentiation efficiency and the overall cell morphology in each lineage were not affected by LSD1^{MUT}, consistent with comparable expression levels of lineage-specific marker genes (Extended Data Fig. 3d) and suggesting that the decreased expression of cell cycle genes is not caused by developmental defects.
The downregulation of genes in differentiated endoderm and neuronal cells observed in LSD1^{MUT} could result from reduced activation of up-regulated genes during differentiation or increased repression of down-regulated genes. To distinguish between these two possibilities, we compared gene expression changes in LSD1^{MUT} and LSD1^{WT} endoderm split into up- and down-regulated genes relative to expression levels in hiPSCs (Extended Data Fig. 3e). This analysis revealed that genes whose expression decreased in LSD1^{WT} endoderm compared to hiPSCs were more strongly downregulated in LSD1^{MUT} endoderm. Given the reduced cell proliferation capacity when transitioning from hiPSCs to defined cell lineages, genes in these categories decreased in expression, but the decrease was stronger in LSD1^{MUT}.

eGRN TF regulons downregulated in LSD1^{MUT} at early lineage differentiation

Our eGRN identified a specific set of TFs (inferred by motif) whose regulons were mis-regulated in LSD1^{MUT} fibroblasts. To determine the effects of LSD1^{MUT} on TF-gene pairs in the other cell types, we performed the TF regulon analysis in LSD1^{MUT} vs LSD1^{WT} hiPSCs and hiPSC-derived cell lineages. Similar to the fibroblast data, most TF regulons were upregulated in LSD1^{MUT} hiPSCs (Fig. 3d), consistent with the LSD1 repressive function. However, during early cell differentiation (from hiPSCs to endoderm, mesoderm, and neuronal lineages) the majority of TF regulons were downregulated in LSD1^{MUT} (Fig. 3d). To analyze the regulons across different lineages, we focused on TFs that were not differentially expressed following differentiation (FDR > 0.1 and absolute log2FC < 0.58) but whose regulon activity was significantly altered in LSD1^{MUT}. This identified 144 TFs, which were then grouped into three classes based on unsupervised clustering of their regulon activity across cell types (Fig. 3e). Cluster 1 contains TFs with upregulated regulon activity in fibroblasts, unaltered in hiPSCs, and downregulated in endoderm, mesoderm, and neuronal lineage in LSD1^{MUT} vs LSD1^{WT}. Cluster 2 TF regulons are downregulated in both fibroblasts and differentiation lineages, and upregulated in hiPSCs.

Cluster 3 TF regulons are not altered in fibroblasts but are downregulated in the differentiated cell lineages. Thus, all TF regulons are repressed by LSD1^{MUT} in the three differentiating lineages, whereas TF regulons are predominantly upregulated by LSD1^{MUT} in fibroblasts and hiPSCs (Fig. 2c and Fig. 3d). Upregulated TF regulons are separated into two distinct sets (clusters 1 and 2), suggesting that LSD1^{MUT} affects TF activity in a cell type-specific manner. The effect size of the repression is the strongest in cluster 2 and overall more substantial in the endoderm (Fig. 3e). Functional enrichment analysis among TF regulons in three Clusters revealed significant overrepresentation of cell proliferation related categories such as DNA replication, translation, and mitotic cell cycle (Extended Data Fig. 3f).

To examine specific TFs (inferred by motif) and their regulons in detail, we selected the top 10 TFs whose regulons were significantly altered in endoderm by LSD1^{MUT} (Fig. 3f). Four of the TFs are chromatin interactors: the autoimmune regulator AIRE selectively binds unmethylated H3K4[19]; transcriptional coactivator ARID5B is involved in histone H3K9me2 de-methylation[20]; BPTF is a histone-binding component of the NURF chromatin remodelling complex, specifically recognizing H3K4me3[21]; and BCL6 is a transcriptional repressor that recruits histone deacetylases[22]. The other six include the developmental regulators SOX11 and DLX1 and the cell cycle regulator HMGA2. The 10 TFs are linked to 158 genes differentially expressed in LSD1^{MUT} endoderm. The majority of these genes (133 genes) are regulated by only one of the 10 TFs (Fig. 3f). Thus, the TFs whose regulons were most affected by LSD1^{MUT} during differentiation may promote the LSD1^{MUT} phenotype due to their diverse interaction with histones or histone-binding proteins and their role in regulating developmental processes.

Additionally, distinct TF regulon clusters could be associated with specific genetic risk factors. To investigate if regulatory regions associated with TF regulon clusters 1-3 are enriched for common genetic traits, we performed linkage disequilibrium score regression (LDSC) analysis[23] using 442 GWAS catalogue traits (Fig. 3g and Methods). The TF regulons of cluster 1 are enriched for immune and blood-related GWAS traits (osteoarthritis, asthma, Crohn’s disease, hemoglobin and basophil counts), suggesting that the inverse TF regulon expression patterns observed in fibroblasts and early differentiation are associated with immune system phenotypes. The TF regulons of cluster 2, down-regulated in all cell types except hiPSCs, are enriched in cardio-vascular and brain related traits (small vessel stroke, pulse pressure, conscientiousness measurement), suggesting these traits are associated with the TF regulons conserved across multiple cell types. The TF regulons of cluster 3, which are down-regulated in early differentiation, are enriched in neurological GWAS traits (social interaction measurement, educational attainment, handedness), consistent with the neurodevelopmental phenotypes of the CPRF patients and indicating the relevance of disease-associated traits to early cell differentiation of patient-derived cell lines.

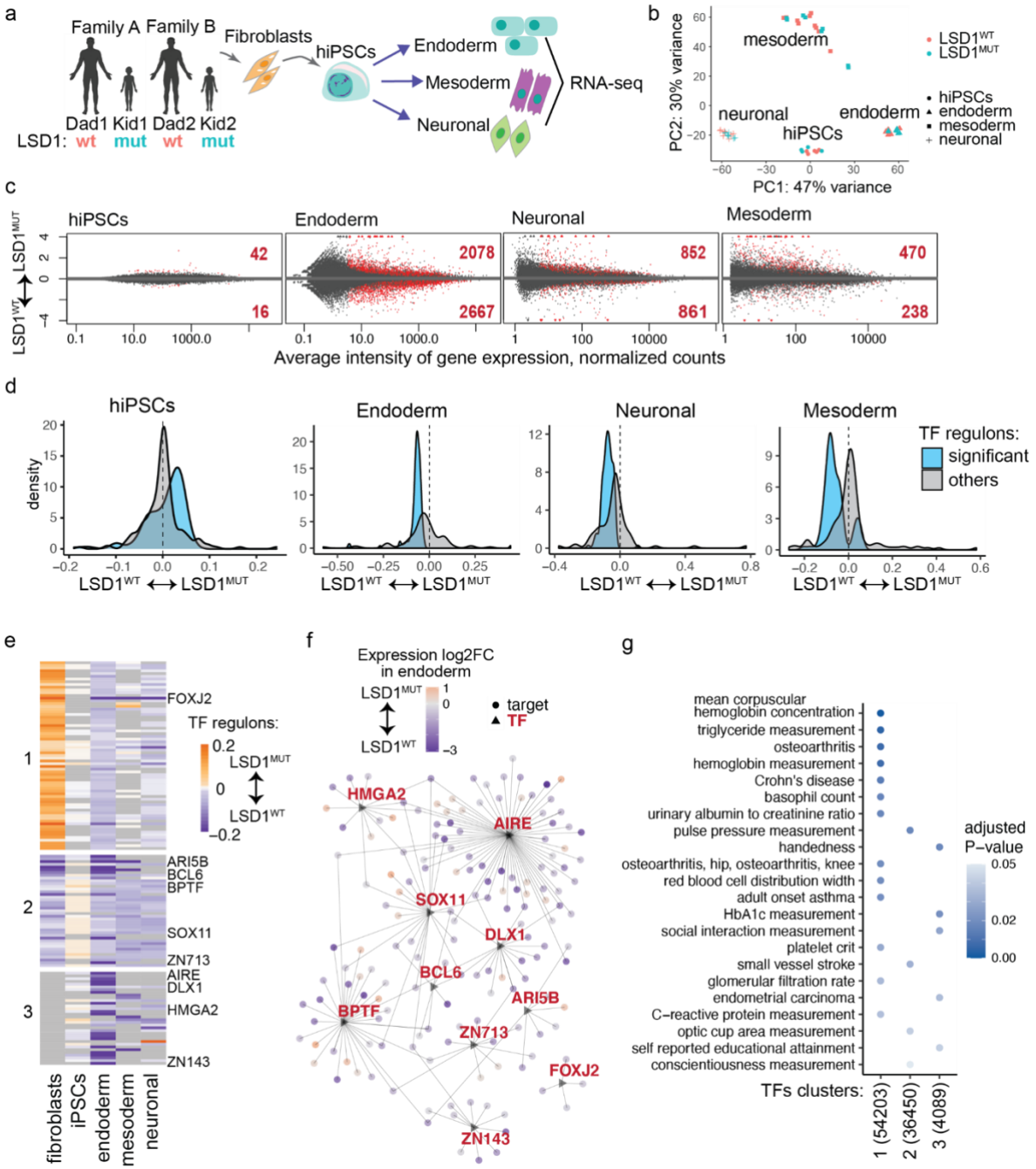

Figure 3. eGRN analysis identifies aberrant gene repression by LSD1^{MUT} during the early differentiation of cell lineages. a) Reprogramming of primary fibroblasts into hiPSCs and subsequent differentiation into three main embryonic lineages. b) Principal component analysis (PCA) plot of RNA-seq data in hiPSCs and derived from them endoderm, neuronal and mesoderm lineages. Principal components 1 and 2 are shown together with the variance they explain. c) Differential expression analysis of LSD1^{MUT} effects on hiPSCs and early differentiation in three embryonic lineages. n=8 for LSD1^{MUT} and n=10 for LSD1^{WT}. d) Density plots of TF regulons expression in LSD1^{MUT} hiPSCs and derived from them endoderm, mesoderm and neuronal lineages. Significant TF targets are upregulated in hiPSCs but downregulated in lineages. e) Heatmap of a GRN subnetwork showing average expression changes of TF regulons in LSD1^{MUT} across cell types. This subnetwork includes 144 TFs that are differentially active and whose targets' expression is significantly changed in LSD1^{MUT} cell lineages. f) Graph representation of an eGRN subset of the 10 TFs, whose regulons were most affected in endoderm differentiation. Only significantly differential TF targets (circles) are shown, colored by their expression log2 fold change in LSD1^{MUT} vs. LSD1^{WT}. g) LDSC analysis results showing significant enrichments of GWAS traits in regulatory regions associated with TF regulons in clusters 1-3, see panel D. Number of regulatory regions is indicated in brackets. Adjusted p-values were calculated within each trait while including all GRN peaks as background.

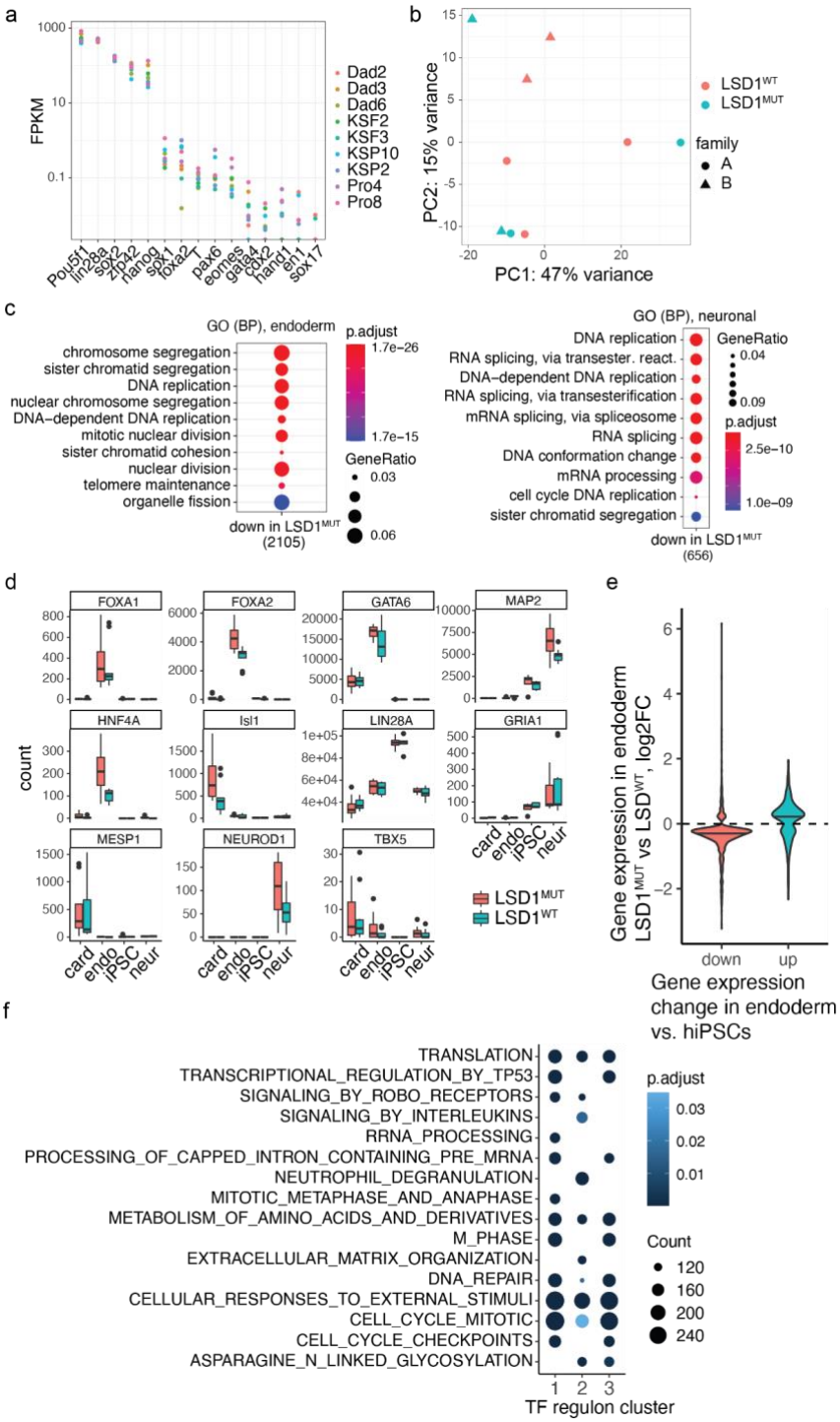

Extended Data Fig.3. a) Expression of pluripotency markers (Pou5f1, Linc28a, Sox2, Nanog) and lineage markers (Sox1, T, Eomes, Foxa2, Pax6) to confirm the successful reprogramming of primary fibroblasts into hiPSCs: induction of pluripotency markers expression and repression of lineage genes. Expression values are shown as FPKMs from the RNA-seq data. Cell lines: $LSD1^{WT}$ - “Dad” (individual from family 1) and “KSF” (individual from family 2), 2-3 clonal lines per individual; $LSD1^{MUT}$ - “Pro” and “KSP”, 2 clonal lines per individual. b) PCA plot of top 300 variable genes in hiPSC lines derived from $LSD1^{MUT}$ and $LSD1^{WT}$ patient samples. c) GO enrichment of significantly differential genes in $LSD1^{MUT}$ lineages, only gene sets with enrichments having adjusted p-value < 0.1 are shown (none for mesoderm lineage). d) Expression of endoderm, mesoderm and neuronal markers in iPSC-derived early differentiated lineages. e) Expression changes of significantly differential genes in $LSD1^{MUT}$ or control endoderm cells, split into two categories: genes up- or down-regulated (by log2FC) in endoderm relative to hiPSCs. The genes are stronger downregulated in $LSD1^{MUT}$ endoderm differentiation compared to control samples. f) gene ontology (GO) enrichment of TF regulons in the three clusters from Fig. 3e.

LSD1^{MUT} increases HDAC activity and repression of target genes

To understand how TF regulons are being repressed in LSD1^{MUT} during early differentiation, we considered two possibilities: a dosage effect and a mutation-specific effect (Fig. 4a). A dosage effect was observed in heterozygous LSD1^{MUT} fibroblasts and hiPSCs, where TF regulons were upregulated due to the reduction in LSD1-mediated repression. The stronger repression of TF regulons seen during early differentiation in LSD1^{MUT} could be caused indirectly, e.g. by overexpression of repressive TFs. Indeed, 14 repressor TFs are upregulated in endoderm, mesoderm, or the neuronal lineage but none of them significantly increased in all three cell types (Extended Data Fig.4a), whereas the global downregulation of TF regulons is found in all three lineages, suggesting that overexpression of repressors does not fully explain the molecular phenotype. A mutation-specific effect is suggested by a previous biochemical study of CPRF patients' mutations[13], which has shown that the LSD1^{MUT} is still able to interact with its repressive co-factors (HDACs and the Co-REST complex) and, to some extent, histone substrates. Because many LSD1 co-factors have a repressive role, their increased recruitment and/or activity in LSD1^{MUT} cells could lead to the decrease in histone acetylation and observed over-repression of TF regulons (Fig. 4a).

To further characterize the dosage and mutation-specific effects we used RNA-seq to analyze normal hiPSCs treated with either a chemical inhibitor of LSD1 (acutely, for 24h, or chronically, for 7 days) or shRNA to knock-down LSD1 (see Methods). Comparing gene expression changes arising from these perturbations (reduced dosage of LSD1) with the LSD1^{MUT} data from reprogrammed hiPSCs (mutation-specific condition) allowed the identification of dosage and mutation-specific effects (Fig. 4b). Genes that were differentially expressed in any of these conditions grouped into 6 main clusters, with most genes (cluster 1, n=133) being upregulated, given the loss of LSD1 repressive functions (Fig. 4b). The transcriptional repressor Zeb1 was among the upregulated genes, its increased expression potentially resulting in stronger downregulation of its targets and contributing to the phenotype we observed during hiPSCs differentiation (Fig. 3c). The second cluster (n=39 genes) contained genes that were downregulated only in LSD1^{MUT}, suggesting mutation-specific regulation. Assessing HDAC activity from published data on the HDAC substrate H3K27ac in human stem cells (hESCs, see Methods), we found genes in the second cluster were linked to chromatin regions with less H3K27ac signal (Fig. 4c). These results suggest that there is increased HDAC activity in the LSD1^{MUT} cells and not in the cells with reduced dosage of LSD1.

HDAC repression in LSD1^{MUT} reverses altered gene expression

Given the connection between decreased gene expression in LSD1^{MUT} and increased HDAC activity, we hypothesized that chemical inhibition of HDAC activity might rescue repression of the TF regulons during differentiation. To test this, we differentiated hiPSC lines (n= 5, LSD1^{WT}; n = 4, LSD1^{MUT}) into endoderm, treating differentiating cells with the HDAC inhibitor valproic acid (VPA) or vehicle control, and measured changes in gene expression (LSD1^{MUT} vs. LSD1^{WT} cells). VPA, approved by the FDA for the treatment of epilepsy and mood disorders[24], inhibits both class I and class IIa HDACs [25–27], increasing the levels of acetylated histones (Extended Data Fig.4b). In the untreated LSD1^{MUT} endoderm we identified 1170 differentially expressed genes. VPA treatment rescued expression of nearly all of these genes, with only 21 remaining

significantly differentially expressed (Fig. 4d). Most of the genes that were downregulated in $LSD1^{MUT}$ and rescued by VPA treatment were expressed at levels close to $LSD1^{WT}$ levels (Fig. 4e).

To investigate the basis for the highly effective VPA-mediated rescue, we examined the TF regulons and identified the top 30 TF motifs (Extended Data Fig. 4c) that were linked to the genes rescued by VPA. Among them, we observed TFs related to cell proliferation and metabolism (SP1, SP3, SP4, Oct4, Nanog, E2F6, ESR1) and the EMT (Zeb1, Snai2, Twist1). When we assessed all TF motifs linked to genes rescued by VPA, we found a significant enrichment of TFs whose regulons were affected by $LSD1^{MUT}$ in the network-based analysis (Fig. 3d, Fisher's test odds ratio 1.35, p-value = 2e-16). This result suggests that VPA treatment is rescuing the TF regulons impaired by $LSD1^{MUT}$.

To assess the global effects of VPA treatment on TF regulons, we compared the TF regulon expression changes in untreated and VPA-treated $LSD1^{MUT}$ endoderm. We observed significant upregulation of TF regulons and partial rescue of the $LSD1^{MUT}$ effects on global gene expression (Extended Data Fig. 4d). TF regulons whose expression was most rescued by VPA significantly overlapped with the most affected TFs in endoderm differentiation (Fig. 3e), including TFs related to cell growth and differentiation (Erf1, Dlx1, HMGA2), as well as chromatin interacting TFs (AIRE, BCL6 and BPTF, Fig. 3e and 4f). We conclude that the effects of $LSD1^{MUT}$ on early cell differentiation are related to HDAC-mediated over-repression of cell proliferation genes, and likely mediated by a specific group of TFs.

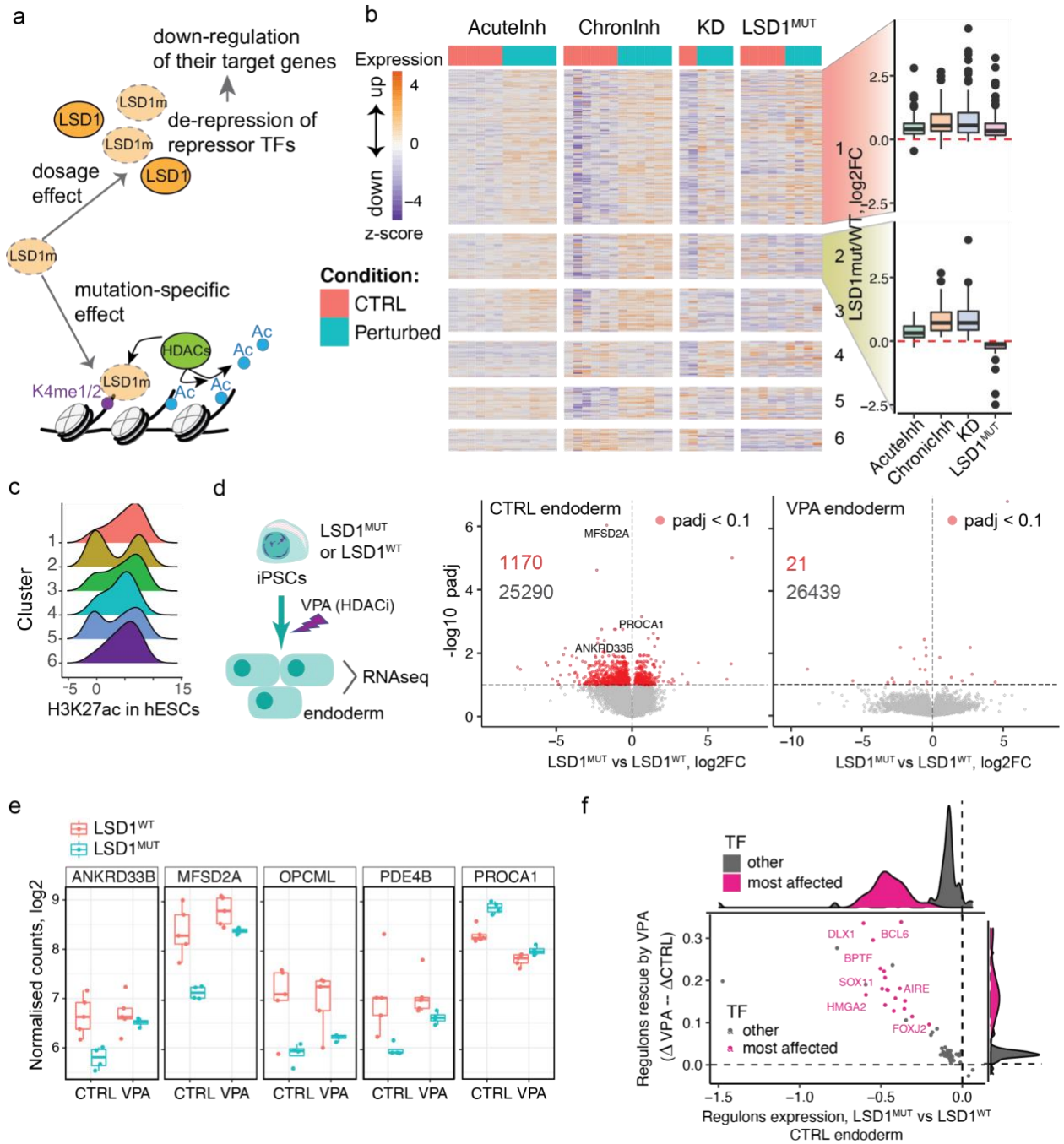

Figure 4. Increased HDAC activity leads to over-repression of TF targets in LSD1^{MUT}. a) Scheme of dosage and mutation-specific effects in LSD1^{MUT}. b) Heatmap of gene expression changes in the control and perturbed hiPSCs (acute or chronic chemical inhibition of LSD1, knockdown of LSD1 by shRNA and CPRF patient-derived cells). Normalized expression values are shown as z-scores within each treatment batch. Boxplots of log2 fold changes between perturbed and control cells in each condition are shown on the right for the two first clusters. c) Density plots of H3K27ac signal in human embryonic stem cells (ENCODE) at regulatory regions linked to the genes in the heatmap on panel B. Cluster 2 shows strong bimodal distribution of low- and high-K27ac regions. d) CPRF patient-derived hiPSCs were differentiated within 48h to endoderm in the presence of HDAC-inhibitor VPA and gene expression was measured by RNA-seq. Volcano plots show the distribution of gene expression changes in LSD1^{MUT} vs LSD1^{WT} control and VPA-treated endoderm. Significantly differential genes (padj < 0.1) are highlighted in red. n=4 for LSD1^{MUT} and n=5 for LSD1^{WT} (same for panel e). e) Expression counts of selected top differentially expressed genes in control and VPA treated endoderm. f) Scatter plot of significantly affected by LSD1^{MUT} TF regulons in control endoderm, showing the difference D in TF regulon expression between LSD1^{MUT} and LSD1^{WT}

control endoderm (X-axis) against the size effect of the VPA-mediated rescue of TF regulon expression (D in VPA - D in control endoderm).

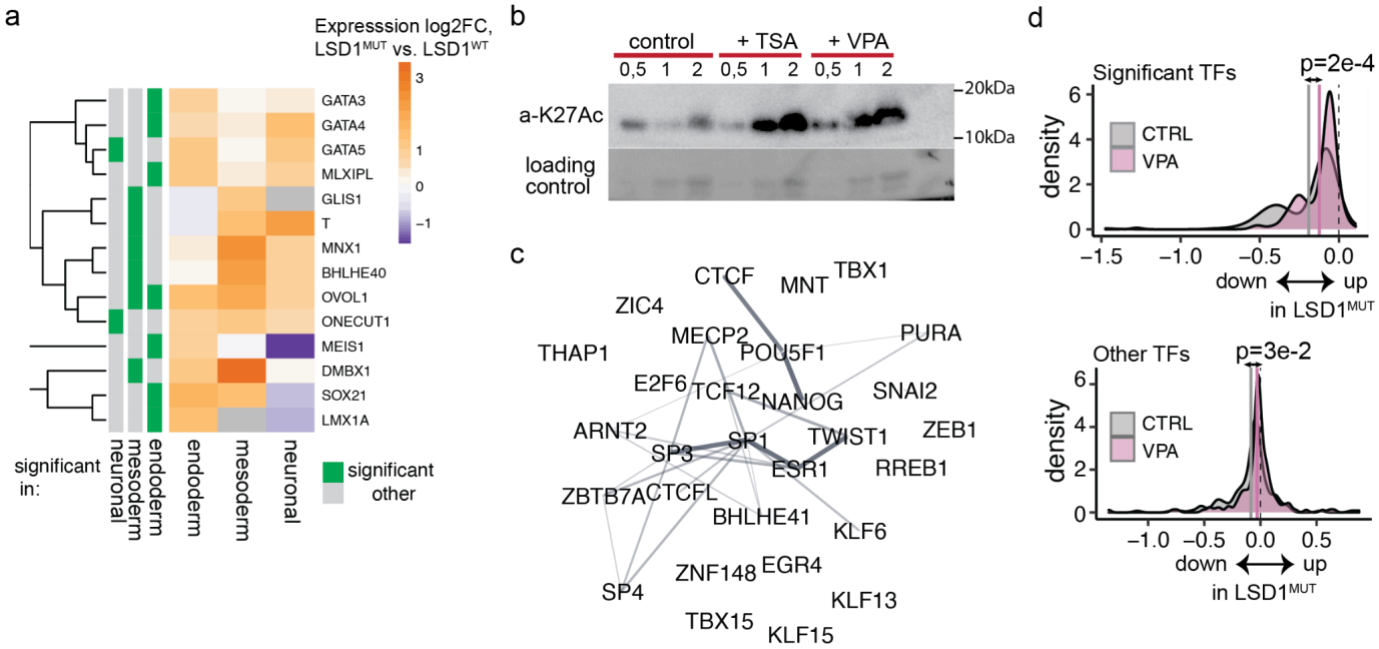

Extended Data Fig. 4. a) TF own expression in differentiation, log2 fold change between LSD1^{MUT} and LSD1^{WT}. Significant expression changes are indicated in green on the left columns. b) Western blot showing increased H3K27ac levels in patient-derived hiPSCs treated with HDAC inhibitors TSA and VPA. c) Top TFs linked to differential genes in control endoderm that were rescued by VPA treatment (TFs ranked by a number of differential genes they are linked to). Connections are experimentally confirmed interactions from the STRING database[28]. d) Distributions of TF regulons expression changes in LSD1^{MUT} vs. LSD1^{WT} in control or VPA-treated endoderm (grey or purple color, respectively). TFs are split into those whose regulons are significantly affected in expression (top plot) or others (bottom plot). Average expression change across all TF regulons in control or VPA-treated endoderm are indicated as dashed vertical lines.

Discussion

De novo point mutations in the histone lysine demethylase LSD1 cause a rare neurodevelopmental disorder, CPRF. However, the molecular mechanisms underlying the disorder are not known. Using CPRF patient-derived primary fibroblasts, hiPSCs and differentiated cell lineages we studied the effects of two different LSD1 mutations on epigenomic and transcriptional landscape, as well as on TF-target gene interactions. We found that in defined cell types (primary fibroblasts and hiPSCs) LSD1^{MUT} leads to the overall upregulation of TF regulons, consistent with a reduction in LSD1 repressive function. In contrast, during the early differentiation of hiPSCs into endoderm, mesoderm and neuronal lineages LSD1^{MUT} had a dominant effect, promoting increased repression of TF regulons, mostly affecting cell proliferation related genes. We have identified HDACs as mediators of the LSD1^{MUT} repressive phenotype and have shown that inhibition of HDAC activity using a chemical compound, VPA, rescues the repressive phenotype in LSD1^{MUT} endoderm differentiation.

LSD1^{MUT} caused changes in activity of a specific set of TFs, as well as expression of their regulons in all analyzed cell types. However, the set of TFs and the direction of the expression

changes of their regulons varied between cell types. Such cell type specific differences could arise from the activity of distinct enhancers in particular cell states[29], or from relocation of LSD1 to different enhancers during cell state transitions. Moreover, interactions of LSD1 with its co-factors and TFs can vary between cell types, for example, through tissue-specific TFs[30], introducing another source of variability in the molecular phenotype of $LSD1^{MUT}$. Sensitivity of a particular set of TFs to $LSD1^{MUT}$ might reflect the susceptibility of TF binding sites to the chromatin environment altered by $LSD1^{MUT}$. Indeed, among the TFs most affected by $LSD1^{MUT}$ during cell differentiation are chromatin-interacting factors AIRE and BPTF, which are sensitive to the methylation state of H3K4 when binding to chromatin, and BCL6, which recruits histone deacetylases.

Our eGRN identified enhancer-mediated TF-target gene connections directly affected by $LSD1^{MUT}$, facilitating the dissection of LSD1 effects into dosage loss of function of LSD1 and dominant effects of $LSD1^{MUT}$. Thus, CPRF molecular pathology cannot be fully dissected using the only loss of function model systems due to substantial mutation-specific transcriptional effects. $LSD1^{MUT}$ has a dominant repressive effect on TF regulon expression during cell differentiation. We show that this effect is linked to HDACs, known LSD1 co-factors. HDAC inhibitors were previously found to rescue a deficiency in KMT2D, an H3K4 methyltransferase, by balancing the lack of active H3K4 marks[31], whereas in this work, the rescue of a repressor LSD1 impairment is achieved by inhibiting another repressor (HDAC), suggesting that HDACs have higher activity or recruitment of in the presence of $LSD1^{MUT}$ protein. In the fibroblast and hiPSC cell states we did not observe increased repression of target genes, suggesting this molecular phenotype might be transient and compensated for later by the wild-type copy of LSD1. Nevertheless, the defects in early cell differentiation could have profound consequences on tissue formation and organism development.

LSD1 demethylation activity is inhibited in the presence of acetylated histones[32], suggesting that acetylation levels at LSD1-bound regions in different cell states (fibroblasts, hiPSCs or during cell differentiation) could influence the effects of $LSD1^{MUT}$. During cell differentiation H3K27ac levels decrease at enhancers of proliferation-related genes[17] (due to reduced p300 recruitment/activity and increased deacetylation by HDACs), enabling LSD1 to demethylate these regions. The inactive $LSD1^{MUT}$ protein results in longer residence times for the LSD1-HDAC complex at its target regions, causing even stronger repression of TF regulons. This effect is only transient and compensated for by the functional $LSD1^{WT}$ copy after differentiation (e.g. in fibroblasts), with the upregulation of TF regulons likely caused by an overall increase in poised enhancers marked by H3K4me1, due to the lack of demethylation activity in $LSD1^{MUT}$ and the associated “aberrant” gene expression.

Overall, we show that $LSD1^{MUT}$ is linked to misregulation of the global chromatin regulatory landscape, which affects motif accessibility of a specific set of TFs and the expression of genes related to cell proliferation, differentiation and development. We also identified a group of TFs whose activity was impaired in a cell-type specific manner by $LSD1^{MUT}$ and have shown that an FDA-approved drug, VPA, can rescue TF regulon expression defects caused by $LSD1^{MUT}$ during cell differentiation, suggesting VPA might provide a potential therapeutic avenue to

explore for treatment of CPRF syndrome patients. Given that LSD1 levels are often increased in various cancers[11,33–35], our discovery of the misregulation of LSD1-HDAC activity in regulatory regions could also contribute to the improvement of anti-cancer therapies.

Methods

Data availability

RNA-seq and ATAC-seq raw data for patient-derived human samples have been submitted and are currently processed by the European GenomePhenome Archive. The accession numbers will be communicated to the editor as soon as we receive them. Restrictions apply to the availability of the raw data (deposition in a controlled access repository) due to reasons of sensitivity of the human samples.
Processed ATAC-seq samples (bigwig genome coverage files, hg19 version) and raw RNA-seq gene counts are deposited at EMBL OwnCloud and can be accessed via following link: https://oc.embl.de/index.php/s/fCAO7QCm2MtOmJx.

Code availability

Custom code used to perform the analyses is available from github: https://github.com/dariabunina/LSD1_mutation_study.

Cell lines and culture conditions

Primary skin fibroblasts were obtained from two male pediatric patients and their healthy fathers under a protocol approved by the Institutional Review Board at Translational Genomics Research Institute (TGen). We have obtained informed consent from all participants. Fibroblasts were cultured at 37 C under 5% CO2 in DMEM media supplemented with 10% fetal bovine serum. hiPSCs were generated from primary fibroblasts using Sendai virus reprogramming kit (ThermoFisher Scientific), yielding 2-3 different clonal lines for each individual. hiPSCs were maintained in Essential 8 (E8) media (LifeTech) on vitronectin coated plates following the manufacturer's instructions. hiPSCs were passaged at least twice after thawing prior to the start of differentiation into endoderm, mesoderm and neuronal lineages. For endoderm differentiation we used a PSC Definitive Endoderm (DE) Induction Kit (Gibco, ThermoFisher Scientific Cat. No. A3062601), cells were collected after 2 days. For mesoderm differentiation we used a PSC cardiomyocyte differentiation kit (ThermoFisher Scientific Cat. No. A29212), cells were collected after 4 days. For neuronal differentiation we used a Gibco PSC neural induction medium (ThermoFisher Scientific Cat. No. A1647801) and cells were collected after 7 days. For the VPA treatment hiPSCs were differentiated to endoderm using a 2-day DE Induction Kit following the manufacturer's instructions and from day 0 of differentiation 400uM VPA (valproic acid sodium salt 98%, Sigma Cat. # P4543-10G) in DMSO was added to cell cultures.

Healthy human hiPSC cell lines for Figure 4 were cultured under feeder-free conditions on plates coated with human-qualified Matrigel (BD Biosciences) diluted 1:40 in mTeSR-1 medium (StemCell Technologies). hiPSCs were passaged upon treatment with Accutase (Sigma) and

resuspending them in mTeSR-1 medium supplemented with 5 µM Y-27632 (Sigma). Six hiPSC lines from 3 different individuals were treated with irreversible LSD1 inhibitor DDP26095 (10 uM), produced by the IEO Drug Discovery Unit–Drug Development Program (IEO DDU-DDP), for 24 h (acute inhibition) or 7 days (chronic inhibition). To induce a constitutive knock-down of LSD1, hiPSC lines were transduced with two different validated pLKO.1 TRC vectors containing shRNAs (sh1 (GCTACATCTTACCTTAGTCAT, Clone Cat. N. TRCN0000046071), sh2 (CCACGAGTCAAACCTTTATTT, Clone Cat. N. TRCN0000046072) against *kdm1a* and maintained with mTeSR-1 medium with puromycin (1 ug/ml) for selection. A pLKO.1 TRC vector containing a scrambled short hairpin sequence was used as a negative control.

Chromatin accessibility analysis by ATAC-seq

ATAC-seq experiment was performed on fresh fibroblasts in 2 biological replicates per individual according to published protocol[36]. Briefly, 50.000 cells were harvested and washed once in cold PBS for 5 min at 500 g at 4C. The pellet was gently resuspended in 50ul of cold lysis buffer containing 0.1% NP-40 and immediately spun down at 500 g for 10 min at 4 C. Transposition reaction mix containing transposition buffer and 2.5 ul of Tn5 enzyme per sample (Illumina) was added to the pellet and incubated for 30 min at 37 C. The reaction was stopped and DNA was purified using a Qiagen MinElute kit and eluted in 10ul of the EB buffer. DNA was PCR amplified for a total of 11-13 cycles using barcoded primers (Illumina Nextera XT Index Kit v2) and purified using Ampure beads (1.4:1 beads:sample ratio). The quality and concentrations of the eluted libraries was determined using an Agilent Bioanalyzer HS chip. Libraries were sequenced on Illumina NextSeq500 in paired-end mode.

ATAC-seq data analysis

ATAC-seq data were processed following the steps in[37] using the custom Snakemake[38] pipeline. Briefly, reads were trimmed using Trimmomatic[39] and aligned to the human genome (hg19) using Bowtie2 with parameters -X 2000 --very-sensitive. The read start sites were adjusted due to the transposon insertion specifics of Tn5. Mitochondrial reads and duplicated reads were removed with Picard tools, peak calling was performed using macs2 with parameters --nolambda --nomodel --slocal 10,000.
To look for differentially accessible regions a consensus peak set using samples from all individuals and replicates was produced using the R package DiffBind (minimum of 2 samples to retain a peak), resulting in 96,467 peaks. The accessibility signal was corrected with loess and significantly differentially accessible regions were defined by an FDR threshold of 0.05.

ChromHMM analysis (for Extended Data Fig.1b). To analyze the distribution of differential ATAC-seq peaks across different chromatin states we downloaded a 15-state core ChromHMM model (computed on foreskin fibroblast data, cell type E055) https://egg2.wustl.edu/roadmap/web_portal/chr_state_learning.html. The enrichments of peaks (differential peaks more accessible in $LSD1^{MUT}$ or less accessible in $LSD1^{MUT}$ and non-differential peaks) were calculated using the ChromHMM software v.1.22 using the OverlapEnrichment command and default settings http://compbio.mit.edu/ChromHMM/.

TF activity analysis

Differential TF activity between LSD1^{MUT} and LSD1^{WT} was analysed as in[40] using diffTF tool[14]. Briefly, this method uses predicted TF binding sites defined by a genome-wide PWM scanner and overlaps these with accessible chromatin in ATAC-seq peaks. As a PWM database source, we used Jaspar CORE 2018 database (Khan et al., 2018), extended TF binding sites by 50 bp in each direction and calculated a fold change in ATAC-seq reads between LSD1^{MUT} and LSD1^{WT} conditions, such that the final TF activity value for each TF corresponds to the mean of genome-wide differences in accessibility at the TF's binding sites between the conditions. Statistical significance was calculated as a Cohen's distance of the weighted mean differences distribution to the matching distribution calculated for a permuted binding site of the corresponding TF. Gene ontology analysis on significant TFs was performed using clusterProfiler R package[41] and all TFs as a background.

Ageing-related TFs (as well as other genes in the subsequent RNA-seq analysis of the fibroblast data) were excluded from the fibroblasts analysis. The lists of ageing-related genes were taken from a curated database of human ageing genes GenAge https://genomics.senescence.info/genes/allgenes.php and from a list of genes whose expression was found significantly differential in ageing skin[42].

Gene expression profiling by RNA-seq

Samples for all RNA-seq experiments in this work were collected in two biological replicates from each of 2-3 clonal lines or individuals in case of primary fibroblasts (except for the VPA-treated endoderm where individual cell lines were used as biological replicates). RNA was isolated from 600.000-1.200.000 snap-frozen cell pellets using Qiagen RNeasy Mini kit and treated with TURBO DNA-free kit (Ambion) to remove DNA. The quality of RNA was verified on Agilent Bioanalyzer. 1ug of total RNA was used as input for poly-A selection (NEBNext PolyA mRNA magnetic isolation module), cDNA synthesis and library preparation with NEBNext Ultra RNA Library Prep Kit for Illumina according to the manufacturer's instructions. Library quality was determined using Agilent Bioanalyzer and concentration was measured by Qubit fluorometer. Libraries were sequenced on Illumina NextSeq500 in single-end mode.
RNA-seq reads were adapter trimmed using Trimmomatic and aligned to the human genome (hg19) with STAR aligner version 2.5.2b https://github.com/alexdobin/STAR using default parameters. Gene counts were produced with a summarizeOverlaps function from the GenomicAlignments R package and Gencode version 19 annotation of all human genes. Differential expression analysis was performed using an R package DESeq2[43] in each cell type separately (fibroblasts, hiPSCs, differentiating endoderm or mesoderm or neuronal cells) between LSD1^{MUT} and LSD1^{WT} cell lines. Fibroblasts: samples from primary cell cultures of two individuals grown in two different flasks were used as biological replicates (2x2=4 replicates per condition); iPSCs and VPA-treatment endoderm: 2-3 clonal lines derived from each individual were used as biological replicates; untreated endoderm and mesoderm and neuronal lineages: 2-3 clonal lines derived from each individual were grown in two flasks each and used as biological replicates(LSD1^{MUT}: 2 x 2flasks x 2individuals = 8 replicates, LSD1^{WT}: 2 x 2flasks x 1individual + 3 x 2flasks x 1individual = 10 replicates). Significantly differential genes were defined by adjusted p-value cutoff < 0.1.

Gene ontology enrichment analyses were done with clusterProfiler R package[41] using MSigDB database of Reactome-Kegg pathways or "Biological process" GO annotation, p-adjusted cutoff < 0.1.

Integration of RNA-seq data of LSD1 inhibition and knock-down of normal hiPSCs

Differential gene expression analysis on all hiPSC samples (from the RNA-seq experiments on patient-derived hiPSCs, as well as on normal hiPSC lines treated with LSD1 inhibitor or sh-RNA against LSD1) was performed using edgeR package[44] and glmRLT function with a model.matrix(~experiment+condition2), where "experiment" refers to $LSD1^{MUT}$/LSD1inhibition/LSD1knockdown and "condition2" is control samples vs. any of the perturbations. Significantly differential genes in at least one of the conditions were defined by FDR < 0.05. For clustering, the edgeR log fold changes per condition were then sqrt-transformed (i.e. `sign(x)*sqrt(abs(x))`) to reduce the impact of a few very large fold changes, and clustered using cluster::clara with k=8. Two of the clusters were merged based on visual similarity and one cluster was not included in the visualization due to the very low number of genes it contained (only two genes), which resulted in 6 final clusters on Fig 4b.

Integration of publicly available H3K27ac ChIP-seq data

To estimate the levels of histone acetylation at the iPSC state across different gene clusters from Fig. 4b we downloaded raw H3K27ac ChIP-seq data of a matching cell type (human embryonic stem cells, cell line H1) from the Roadmap Epigenomics Project https://www.ncbi.nlm.nih.gov/sra/SRX012366[accn]. The raw sequences were adapter trimmed (using Trimmomatic v.0.33[39]) and aligned to hg19 using bowtie2 (v.2.3.2[45]) with parameters -X 2000 -t. We then calculated the levels of H3K27ac at the enhancers linked to the genes in six clusters from Fig. 4b using the DiffBind R package (version 3.0.15[46]), which we visualized as density plots in Fig. 4c.

Gene regulatory network analysis

Gene regulatory network was constructed from the matched RNA-seq and ATAC-seq data of healthy human samples and cell lines described in Table 1 using an unpublished R package https://grp-zaugg.embl-community.io/grn/index.html (Kamal *et al, in preparation*). The studies were selected to include relevant cell types for the CPRF syndrome (brain tissues, differentiation time course of pluripotent stem cells, mesoderm lineage) and have paired RNA-seq and ATAC-seq data from the same samples of normal cells or tissues (unmutated/unperturbed). Raw input data was downloaded from the original publications and uniformly processed with the same pipelines for RNA-seq and ATAC-seq processing, as the fibroblast data described above. The resulting consensus set of ATAC-seq peaks across all 63 samples (peaks retained in the final peakset if they were identified in at least 2 samples) includes 500,000 peaks and counts within this consensus peakset were used as input for the network construction.

The computational approach to construct a gene regulatory network consists of two steps: building TF-enhancer links and enhancer-gene links. The details of this approach are described in[15]. Briefly, in the first step the expression of each TF was correlated with accessibility of each of the enhancer regions (=ATAC-seq peak) with and without a known binding site of the TF (foreground and background, respectively). Known binding sites were defined using the HOCOMOCO database v.10. Significantly correlated TF-enhancer links were identified using empirical FDR of 20% (calculated separately for each TF) and an absolute correlation Pearson's coefficient > 0.4. In the second step chromatin accessibility at the ATAC-seq peaks was correlated with the expression of all genes < 500kb away from the peak and peak-gene links were retained if they were positively and significantly ($P < 0.05$) correlated (our assumption is that accessibility at the regulatory region positively correlates with expression of the linked gene), and if their Pearson's correlation coefficient was > 0.4. This approach resulted in a total of 1.3 million TF-enhancer-gene links, connecting 393 TFs with 15,128 unique genes via 96,050 unique ATAC-seq peaks.

TF regulons expression analysis in $LSD1^{MUT}$ vs. $LSD1^{WT}$ cells

TF regulons were defined as all TF-gene links of each TF within the network. To identify which TF regulons were affected by $LSD1^{MUT}$ we calculated aggregated mean expression log2 fold change of each TF regulon in $LSD1^{MUT}$ vs. $LSD1^{WT}$ and tested whether it differs significantly from all expressed genes (background) in the corresponding cell type (two-sided Student's t-test). The raw p-values from the test were corrected for multiple testing using Benjamini-Hochberg approach and TFs which passed the FDR < 0.1 were defined as having significantly affected regulons (Fig. 2c and 3d, Extended Data Fig. 2a). The difference in means between TF regulons and background genes' expression was further used in the scatter/density plots and in the heatmap (Fig. 2d and 3d-e).

In the VPA treatment experiment significantly affected TF regulons were defined in untreated endoderm and their expression was calculated in VPA-treated samples, preserving the classification into significant and other TFs to keep the comparison between the same sets of TFs before and after treatment.

LDSC analysis

We performed stratified LDSC (S-LDSC[23]) to identify if any of the TF clusters were enriched for heritability in GWAS traits. GWAS summary statistics for 806 traits that included participants of European descent were downloaded from the GWAS catalog (https://www.ebi.ac.uk/gwas/) and harmonized. The summary statistics were converted into the LDSC format as described on the LDSC github repository (https://github.com/bulik/ldsc). Summary statistics with fewer than 10,000 individuals or less than 100,000 genetic markers were removed, leaving 442 GWAS traits. We downloaded 54 sets of genomic features from the Alkes Group public repository (https://alkesgroup.broadinstitute.org/LDSCORE/) to serve as a baseline for the enrichment analyses as described (22). Peak sets were created by taking the enhancer regions of the full LSD1 GRN, as well as the enhancer regions connected to the TFs of clusters 1-3 and those connected to the top 10 TFs for the neuronal, endoderm and mesoderm lineages. The peak set

for the full LSD1 GRN was added to the background regions, while the other enhancer regions were tested for enrichment of heritability. The LDSC enrichment P-values were corrected for multiple testing within each trait using the Benjamini Hochberg method.

Immunoblotting

Cell lysates were separated on precast 4–12% Bis-Tris SDS-PAGE gels (Thermo) in MES buffer and transferred onto nitrocellulose membranes. The blots were incubated with primary antibodies overnight at 4^0 C and for 1 hour at RT with HRP-conjugated secondary antibody. Membranes were developed using the Immobilion Western Chemiluminescence HRP substrate (Millipore). In this work we used the following antibodies: LSD1 - Santa Cruz, # sc-271720;
H3K27ac - Active Motif, #39133; H4 - abcam, # ab10158.

Acknowledgments

We thank the staff at the EMBL Sequencing Core Facility for sample preparations and data generation. We thank Nichole Diaz for reprogramming fibroblasts and differentiating hiPSCs and Guy Riddihough for the critical feedback on this manuscript. D.B. was supported by a fellowship from the EMBL Interdisciplinary Postdoc (EIPOD) programme under Marie Sklodowska-Curie Actions COFUND (grant agreement number 664726). This work is supported by the DFG fund (SPP 1738 to K.M.N.).

Author contributions

D.B., J.B.Z and K.-M.N. conceived the study. J.B.Z and K.-M.N. jointly supervised the study. D.B. performed ATAC-seq and RNA-seq experiments under the supervision of K.-M.N. P.-L.G., A.L.T. and A.Ad. performed LSD1 inhibition and knock-down experiments in healthy hiPSCs, generated and analysed resulting RNA-seq data under the supervision of G.T. N.F.-N.M. helped with cell culture and performed Western Blotting experiments under the supervision of K.-M.N. A.Ah. performed gene expression analysis on LSD1 differentiations and processed input data for the eGRN construction under the supervision of D.B. and J.B.Z. C.A. helped with eGRN analysis, A.C. and M.C.L. performed LDSC analysis under the supervision of J.B.Z. D.B. conducted all other pre- and post-processing computational analyses, data integrations and visualizations under the supervision of J.B.Z. and K.-M.N. S.R. and V.N. obtained primary patient samples with the help of P.L. and K.M.P. D.B., K-M.N. and J.B.Z wrote the manuscript, with the input and approval of all co-authors.

Competing Interests statement

The authors declare no competing interests.

References

1. Wang, P. *et al.* Global analysis of H3K4 methylation defines MLL family member targets and points to a role for MLL1-mediated H3K4 methylation in the regulation of transcriptional initiation by RNA polymerase II. *Mol. Cell. Biol.* **29**, 6074–6085 (2009).
2. Faucher, D. & Wellinger, R. J. Methylated H3K4, a transcription-associated histone modification, is involved in the DNA damage response pathway. *PLoS Genet.* **6**, (2010).
3. Sha, Q.-Q. *et al.* CFP1 coordinates histone H3 lysine-4 trimethylation and meiotic cell cycle progression in mouse oocytes. *Nat. Commun.* **9**, 3477 (2018).
4. Sze, C. C. *et al.* Histone H3K4 methylation-dependent and -independent functions of Set1A/COMPASS in embryonic stem cell self-renewal and differentiation. *Genes Dev.* **31**, 1732–1737 (2017).
5. Shi, Y. *et al.* Histone demethylation mediated by the nuclear amine oxidase homolog LSD1. *Cell* **119**, 941–953 (2004).
6. Humphrey, G. W. *et al.* Stable histone deacetylase complexes distinguished by the presence of SANT domain proteins CoREST/kiaa0071 and Mta-L1. *J. Biol. Chem.* **276**, 6817–6824 (2001).
7. Wang, Y. *et al.* LSD1 is a subunit of the NuRD complex and targets the metastasis programs in breast cancer. *Cell* **138**, 660–672 (2009).
8. Wang, J. *et al.* Opposing LSD1 complexes function in developmental gene activation and repression programmes. *Nature* **446**, 882–887 (2007).
9. Wang, J. *et al.* The lysine demethylase LSD1 (KDM1) is required for maintenance of global DNA methylation. *Nat. Genet.* **41**, 125–129 (2009).
10. Kerenyi, M. A. *et al.* Histone demethylase Lsd1 represses hematopoietic stem and progenitor cell signatures during blood cell maturation. *elife* **2**, e00633 (2013).
11. Amente, S., Lania, L. & Majello, B. The histone LSD1 demethylase in stemness and cancer transcription programs. *Biochim. Biophys. Acta* **1829**, 981–986 (2013).
12. Chong, J. X. *et al.* Gene discovery for Mendelian conditions via social networking: de novo variants in KDM1A cause developmental delay and distinctive facial features. *Genet. Med.* **18**, 788–795 (2016).
13. Pilotto, S. *et al.* LSD1/KDM1A mutations associated to a newly described form of intellectual

disability impair demethylase activity and binding to transcription factors. *Hum. Mol. Genet.* **25**, 2578–2587 (2016).

14. Berest, I. *et al.* Quantification of Differential Transcription Factor Activity and Multiomics-Based Classification into Activators and Repressors: diffTF. *Cell Rep.* **29**, 3147-3159.e12 (2019).
15. Reyes-Palomares, A. *et al.* Remodeling of active endothelial enhancers is associated with aberrant gene-regulatory networks in pulmonary arterial hypertension. *Nat. Commun.* **11**, 1673 (2020).
16. Lai, M. C. *et al.* Enhancer-priming in ageing human bone marrow mesenchymal stromal cells contributes to immune traits. *BioRxiv* (2021) doi:10.1101/2021.09.03.458728.
17. Whyte, W. A. *et al.* Enhancer decommissioning by LSD1 during embryonic stem cell differentiation. *Nature* **482**, 221–225 (2012).
18. Bock, C. *et al.* Reference Maps of human ES and iPS cell variation enable high-throughput characterization of pluripotent cell lines. *Cell* **144**, 439–452 (2011).
19. Koh, A. S., Kingston, R. E., Benoist, C. & Mathis, D. Global relevance of Aire binding to hypomethylated lysine-4 of histone-3. *Proc Natl Acad Sci USA* **107**, 13016–13021 (2010).
20. Hata, K. *et al.* Arid5b facilitates chondrogenesis by recruiting the histone demethylase Phf2 to Sox9-regulated genes. *Nat. Commun.* **4**, 2850 (2013).
21. Li, H. *et al.* Molecular basis for site-specific read-out of histone H3K4me3 by the BPTF PHD finger of NURF. *Nature* **442**, 91–95 (2006).
22. Zhang, H., Okada, S., Hatano, M., Okabe, S. & Tokuhisa, T. A new functional domain of Bcl6 family that recruits histone deacetylases. *Biochimica et Biophysica Acta (BBA) - Molecular Cell Research* **1540**, 188–200 (2001).
23. Finucane, H. K. *et al.* Partitioning heritability by functional annotation using genome-wide association summary statistics. *Nat. Genet.* **47**, 1228–1235 (2015).
24. Sixto-López, Y., Bello, M. & Correa-Basurto, J. Exploring the inhibitory activity of valproic acid against the HDAC family using an MMGBSA approach. *J. Comput. Aided Mol. Des.* **34**, 857–878 (2020).
25. Gurvich, N., Tsygankova, O. M., Meinkoth, J. L. & Klein, P. S. Histone deacetylase is a target of valproic acid-mediated cellular differentiation. *Cancer Res.* **64**, 1079–1086 (2004).

26. Göttlicher, M. *et al.* Valproic acid defines a novel class of HDAC inhibitors inducing differentiation of transformed cells. *EMBO J.* **20**, 6969–6978 (2001).
27. Phiel, C. J. *et al.* Histone deacetylase is a direct target of valproic acid, a potent anticonvulsant, mood stabilizer, and teratogen. *J. Biol. Chem.* **276**, 36734–36741 (2001).
28. Szklarczyk, D. *et al.* STRING v11: protein-protein association networks with increased coverage, supporting functional discovery in genome-wide experimental datasets. *Nucleic Acids Res.* **47**, D607–D613 (2019).
29. Heinz, S., Romanoski, C. E., Benner, C. & Glass, C. K. The selection and function of cell type-specific enhancers. *Nat. Rev. Mol. Cell Biol.* **16**, 144–154 (2015).
30. Yokoyama, A. *et al.* Identification of myelin transcription factor 1 (MyT1) as a subunit of the neural cell type-specific lysine-specific demethylase 1 (LSD1) complex. *J. Biol. Chem.* **289**, 18152–18162 (2014).
31. Bjornsson, H. T. *et al.* Histone deacetylase inhibition rescues structural and functional brain deficits in a mouse model of Kabuki syndrome. *Sci. Transl. Med.* **6**, 256ra135 (2014).
32. Shi, Y.-J. *et al.* Regulation of LSD1 histone demethylase activity by its associated factors. *Mol. Cell* **19**, 857–864 (2005).
33. Theisen, E. R. *et al.* Reversible inhibition of lysine specific demethylase 1 is a novel anti-tumor strategy for poorly differentiated endometrial carcinoma. *BMC Cancer* **14**, 752 (2014).
34. Schulte, J. H. *et al.* Lysine-specific demethylase 1 is strongly expressed in poorly differentiated neuroblastoma: implications for therapy. *Cancer Res.* **69**, 2065–2071 (2009).
35. Hayami, S. *et al.* Overexpression of LSD1 contributes to human carcinogenesis through chromatin regulation in various cancers. *Int. J. Cancer* **128**, 574–586 (2011).
36. Buenrostro, J. D., Wu, B., Chang, H. Y. & Greenleaf, W. J. ATAC-seq: A Method for Assaying Chromatin Accessibility Genome-Wide. *Curr. Protoc. Mol. Biol.* **109**, 21.29.1-21.29.9 (2015).
37. Buenrostro, J. D., Giresi, P. G., Zaba, L. C., Chang, H. Y. & Greenleaf, W. J. Transposition of native chromatin for fast and sensitive epigenomic profiling of open chromatin, DNA-binding proteins and nucleosome position. *Nat. Methods* **10**, 1213–1218 (2013).
38. Köster, J. & Rahmann, S. Snakemake--a scalable bioinformatics workflow engine. *Bioinformatics*

28, 2520–2522 (2012).

39. Bolger, A. M., Lohse, M. & Usadel, B. Trimmomatic: a flexible trimmer for Illumina sequence data. *Bioinformatics* **30**, 2114–2120 (2014).
40. Bunina, D. *et al.* Genomic Rewiring of SOX2 Chromatin Interaction Network during Differentiation of ESCs to Postmitotic Neurons. *Cell Syst.* **10**, 480-494.e8 (2020).
41. Yu, G., Wang, L.-G., Han, Y. & He, Q.-Y. clusterProfiler: an R package for comparing biological themes among gene clusters. *OMICS* **16**, 284–287 (2012).
42. Glass, D. *et al.* Gene expression changes with age in skin, adipose tissue, blood and brain. *Genome Biol.* **14**, R75 (2013).
43. Love, M. I., Huber, W. & Anders, S. Moderated estimation of fold change and dispersion for RNA-seq data with DESeq2. *Genome Biol.* **15**, 550 (2014).
44. Robinson, M. D., McCarthy, D. J. & Smyth, G. K. edgeR: a Bioconductor package for differential expression analysis of digital gene expression data. *Bioinformatics* **26**, 139–140 (2010).
45. Langmead, B. & Salzberg, S. L. Fast gapped-read alignment with Bowtie 2. *Nat. Methods* **9**, 357–359 (2012).
46. Ross-Innes, C. S. *et al.* Differential oestrogen receptor binding is associated with clinical outcome in breast cancer. *Nature* **481**, 389–393 (2012).